

RSC Advances

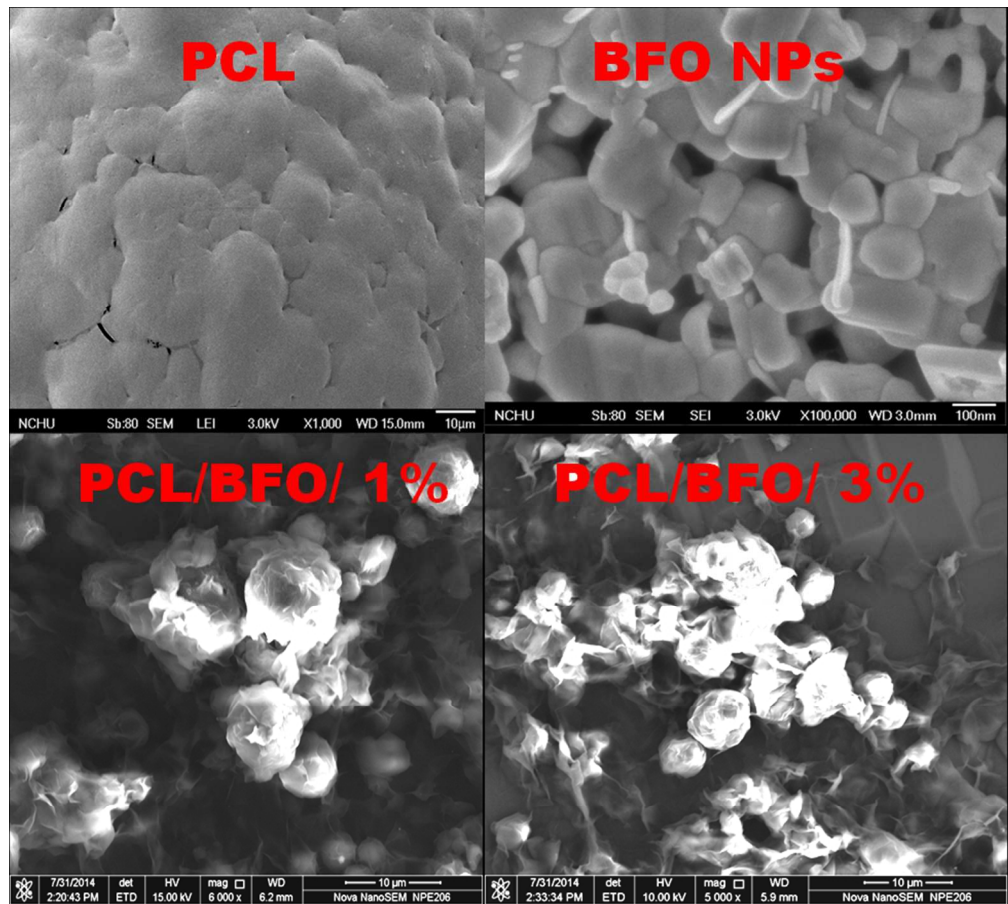


This is an *Accepted Manuscript*, which has been through the Royal Society of Chemistry peer review process and has been accepted for publication.

Accepted Manuscripts are published online shortly after acceptance, before technical editing, formatting and proof reading. Using this free service, authors can make their results available to the community, in citable form, before we publish the edited article. This *Accepted Manuscript* will be replaced by the edited, formatted and paginated article as soon as this is available.

You can find more information about *Accepted Manuscripts* in the [Information for Authors](#).

Please note that technical editing may introduce minor changes to the text and/or graphics, which may alter content. The journal's standard [Terms & Conditions](#) and the [Ethical guidelines](#) still apply. In no event shall the Royal Society of Chemistry be held responsible for any errors or omissions in this *Accepted Manuscript* or any consequences arising from the use of any information it contains.



164x147mm (150 x 150 DPI)

Cite this: DOI: 10.1039/c0xx00000x

www.rsc.org/xxxxxx

ARTICLE TYPE

Solvent-free ring opening polymerization of ϵ -caprolactone and electrical properties of polycaprolactone blended BiFeO_3 nanocomposites†

Somasundaram Saravanamoorthy^a, Muniyandi Muneeswaran^b, NambiVenkatesan Giridharan^b, Sivan Velmathi^{a*}

Received (in XXX, XXX) XthXXXXXXXXXX 20XX, Accepted Xth XXXXXXXXXXXX 20XX

DOI: 10.1039/b000000x

A novel two-phase polymer nanocomposite comprising the polycaprolactone (PCL) and nanocrystalline multiferroic BiFeO_3 (BFO NPs) has been fabricated by the simple casting technique. We have developed a new Schiff base ligand-Ti(IV) catalyst based on tridentate ONO chiral amino alcohol, which has been derived from salicylaldehyde. This catalyst plays a vital role in the ring opening polymerization (ROP) of cyclic ester such as ϵ -caprolactone (ϵ -CL). The nanocomposites consisting of multiferroic BFO NPs and insulating PCL has been prepared. It has been found that the prepared nanocomposite PCL/BFO/1wt%, PCL/BFO/3wt% exhibits the ferroelectric properties and reduced leakage current density. Dielectric data were analyzed using the complex permittivity and complex electric modulus for nanocomposites at room temperature. An improved AC conductivity for PCL/BFO nanocomposites has been observed compared to the pure PCL and BFO sample.

Introduction

Recently much effort has been devoted for synthesizing polycaprolactone (PCL), not only because of its immense applications in the field of medicine and also for its versatile properties in agriculture¹ and material science.² Synthetic polymers have become an indispensable part in daily-life of human beings and the biodegradable class of polymers holds the immense value in therapeutics.³ Among the commercially viable polymers, PCL is an important polymer due to its mechanical properties, biodegradability and for its miscibility with a large range of other polymers.⁴ We can list the promising applications of PCL in medicine and tissue engineering as its took part in drug delivery media for the controlled release of drugs and scaffolds. This plays an important role in the delivery of antibodies and genes,⁵ and also in the development of efficient catalytic systems. Owing to these applications, the preparation of PCL has drawn much attention in both academia and industry. The prime method to synthesize PCL is the ring opening polymerization (ROP) of ϵ -caprolactone (ϵ -CL) with the metal alkoxides as initiators. ROP can be classified based on the usage of solvent into (i) solution polymerization and (ii) solvent-free (bulk) polymerization. Among these two, bulk polymerization is preferred more because

of the following advantages: (i) no requirement of solvent (ii) less vulnerability to impurity levels and unwanted side reactions and (iii) large-scale industrial production.⁶ Most of the solvent-free bulk methods shows improved selectivity, reduced reaction time, and simplified separation and purification of products.⁷ It is remarkable to note that the polyesters prepared using this method have high commercial value as they exhibit good mechanical strength, high crystallinity, biodegradability and adaptable functionalization possibility. Well-defined metal catalysts or initiators has been reported for ROP, including aluminium,⁸ titanium,⁹ tin,¹⁰ zinc¹¹ and magnesium¹² complexes supported by various ligands.

The catalyst gives the polymers with high molecular weights in high yields. Among the above mentioned complexes, titaniumalkoxide based initiator systems seems to be very active and suitable for preparing the PCL due to its high Lewis acidity. However, when metal alkoxides were being used as initiators for ROP of lactones and lactides, this leads to undesirable back-biting and transesterification reactions. This results in macrocycles, catalyst inhomogeneity, and broad or multimodal polymer molecular weight distributions. F. Peruch et al.,¹³ synthesized Ti(IV) complexes of O,N,O-tridentate aminodiols ligands and it has been found that the synthesized Ti(IV) complexes were identified as efficient catalyst for the ROP of L and D,L-lactide in a very controlled manner. Inspired by these results, we postulate that Ti(IV) complex of (S,E)-2-(((1-hydroxy-3-methylbutan-2-yl)imino)methyl)phenol (LVTi) can demonstrate a high catalytic activity in ROP reaction. Catalysis of Schiff-base metal complexes in various chemical reactions both in homogeneous and heterogeneous medium are widely known.¹⁴ The efforts have been laid on their use for ROP are relatively limited.¹⁵ Due to its Lewis acid nature, Ti(IV) complex has been widely used as a catalyst in ROP reactions. Additionally, the transition metal titanium is fairly cheaper than the noble metals like Ag, Ru, Pt, Pd and Au.

Recently, polymer based ferroelectric (FE) materials as like flexible higher particulate ceramic/polymer composites are the crucial components for usages in advanced electronic devices,^{16,17} for instances, memory and gate dielectrics in integrated circuits,

^{18,19} and used as miniature capacitors for telecommunication.^{20–22}

Only a few reports has been focused on the multiferroic properties of the polymer/alloy-based and metal/ceramic based composites. However, due to the large leakage current and easy oxidization, the alloy-based magnetostrictive materials have some extent to, it limitations when being used in nanocomposite. Moreover, a nanoscale structure has its concern on mainly the dielectric and ferroelectric properties of the composites. This results in the main issue for other nanocomposites. And so, their shapes and sizes can also be easily modified by conventional polymeric processing. This helps to increase the electrostriction of the composites. In addition, much FE ceramics contain lead based oxides, which are not environment friendly. Another class of recently discovered interesting ceramic material is the multiferroic materials (MFMs), which have, both magnetic and FE properties. This property drew much attention as a prospective candidate for their potential applications in the emerging fields like information storage, spintronics, and sensor devices.^{23,24} Very recently, it has been noticed that the multiferroic behavior has been observed in the polymer composites consisting of MFMs.^{25,26} BFO is one of the vastly studied MFM system with high FE Curie temperature ($T_C \sim 830$ C).

Polymers prepared using some metal catalysts failed to find industrial application due to their high binding affinity to the polymer, which makes removal of catalyst from polymer difficult. Our objective is to try the catalytic activity of LVTi for ROP of ϵ -Cl under solvent free condition. Also the amount of catalyst used in the present study is very low compared to the results reported in literatures. In this work, we have reported a simple method for the fabrication of new kind of lead (Pb) free materials and low loss PCL/BFO nanocomposites. PCL has been selected as the polymer host for its well-known commercialized applications. PCL is a semicrystalline polymer combines 50% crystalline property with its good mechanical properties, chemical resistance, electrical resistance and processability. Thus we study the electrical properties of BiFeO₃ nanocomposites using the PCL synthesized by our catalyst, as the commercial available PCL is of high cost. In the present study, the catalyst can be removed and recycled thus the metal contamination in the synthesised PCL is very less which is one of the advantages of our article. Our work in this article has been mainly focused on the enhancement of the ferroelectric properties, reduction of the leakage current density and improved AC electrical conductivity by using BFO NPs as suitable multiferroic filler.

2. Experimental

2.1 Materials

L-valine (Merck), iodine (Merck), sodium borohydride (Merck), hexane (Merck), salicylaldehyde (Merck), potassium hydroxide (Rankem), ethanol (Merck), methanol (Rankem), chloroform (Merck), tetrahydrofuran (Rankem), titanium isopropoxide (Sigma Aldrich), 2-popropanol (Merck), ϵ -caprolactone (Sigma Aldrich), bismuth nitrate (Merck), iron(III) nitrate nonahydrate (Merck), ammonium hydroxide (Merck), were used as received. Tetrahydrofuran has been used only after distillation with sodium metal and benzophenone.

2.2 Characterization

The ¹H and ¹³C NMR spectra were recorded by Bruker 400 MHz NMR spectrometer in an appropriate solvent (DMSO-d₆ or CDCl₃) using tetramethylsilane (TMS) as an internal standard. FT-IR spectra were recorded by a Thermo IS5 FT-IR spectrophotometer and wide-angle X-ray diffraction (WAXD) analysis has been done by a Rotaflex RTP300 X-ray diffractometer (RigakuCo., Tokyo, Japan). Shimadzu UV-2600 UV-vis spectrophotometer has been used to record UV-visible spectra using quartz cell with 1 cm path length. The mass spectra were recorded by ESI technique on SYNAPT G2 mass spectrometer instrument. For DSC (differential scanning calorimeter DSC Q10 V9.4 Build 275) analysis, approximately 5–10 mg of the sample was weighed and spread uniformly in a hermetic aluminum pan to ensure proper thermal contact. Microstructure and morphology studies were performed using a field emission scanning electron microscope (Nova NanoSEM NPE 206 high resolution SEM). Dielectric and AC conductivity studies were performed with LCR meter (HIOKI 3532-50, Japan). Leakage measurements were done with Keithley 6517, and ferroelectric studies were performed with P-E loop tracer (Precision II, Multiferroic Tester, Radiant Technologies, USA). The number and weight average molecular weight (M_n and M_w) as well as polydispersity (M_w/M_n) index (PDI) of polymer samples were measured by gel permeation chromatography (GPC) using a Waters HPLC system equipped with a model 515 EF binary pump, model 2707 auto injector, model 2414 refractive index detector (RI), and Waters styragel columns (HR 3 and HR 4). THF (HPLC grade) has been used as an eluent at a flow rate of 1.0 mL/min. The sample concentration and injection volumes were 0.25% (w/v) and 50 μ L respectively. Empower Waters software has been used to calculate molecular weights based on a calibration curve generated by narrow molecular weight distribution of polystyrene standards.

2.2 Synthesis of Ligand

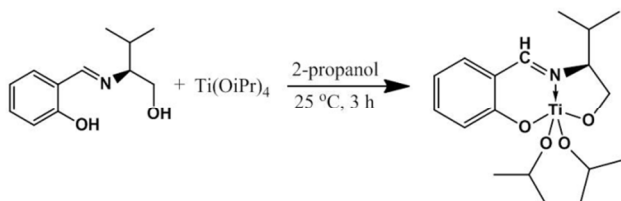
(S)-2-amino-3-methyl-1,1-diphenylbutanol-1-ol (LV) has been synthesized as per the previously reported procedure.^{27,28} The prepared chiral Schiff base was characterized by ¹H NMR, ¹³C NMR and FT-IR respectively.

LV:

Melting point: 99–102°C, $[\alpha]_D^{25} = -24.1^\circ$ ($c = 1$, CH₃OH). FT-IR (cm⁻¹) 3580, 2962, 1628, 1278, 1075. ¹H NMR (CDCl₃, δ ppm): 0.88 (dd, 3J = 1.2 Hz, 6H, -(CH₃)₂), 1.87 (m, 3J = 6.4 Hz, 1H, -CH), 2.99 (m, 3J = 2.8 Hz, 1H, -CH), 3.69 (dd, 3J = 2.4 Hz, 1H, -CH), 3.76 (dd, 3J = 3.6 Hz, 1H, -CH), 5.04 (s, 1H, OH), 6.82 (t, 3J = 6.4 Hz, 1H, -CH), 6.88 (d, 3J = 8.4 Hz, 1H, -CH), 7.19 (t, 3J = 7.6 Hz, 1H, -CH), 7.25 (d, 3J = 7.2 Hz, 1H, -CH), 8.29 (s, 1H, -C=N), 7.8 (s, 1H, -OH). ¹³C NMR (CDCl₃, δ ppm): 17.85, 32.15, 62.1, 79.81, 117.3, 120.5, 123.7, 130.1, 133.6, 151.4, 161.53.

2.3 Preparation of complex:

Ti(OⁱPr)₄ (0.85 g, 3 mmol) in 10 mL of isopropyl alcohol has been cooled to 0°C. Subsequently the required LV (0.618 g, 3 mmol) in 10 mL of isopropyl alcohol has been added drop wise to the reaction mixture with vigorous stirring. The mixture was then stirred at room temperature (25 °C) for 3 h to give a clear orange yellow solution (Scheme 1). The solvent is then removed under vacuum to yield titanium isopropoxide complex as a crystalline orange yellow solid (0.98 g, 88% yield).

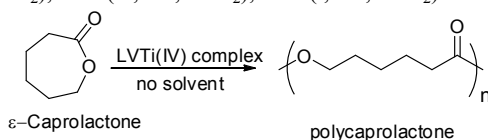


Scheme 1 Synthesis of LVTi Metal complex

Melting point: $>320^{\circ}\text{C}$, $[\alpha]_{\text{D}}^{25} = -125.25$ ($c = 1$, CH_3OH). Mass spectra: molecular ion peak at 370 m/z . ^1H NMR ($\text{DMSO}-d_6$, δ ppm) 0.89 (m, $-\text{CH}_3$), 1.01 (m, $-\text{CH}_3$), 1.05 (m, $-\text{CH}_3$), 1.72 (m, $-\text{CH}_3$), 2.51 (s, $J = 5.9\text{Hz}$, $-\text{CH}$), 3.58 (m, $J = 1.93\text{Hz}$, $-\text{CH}$), 3.88 (d, $J = 2.84\text{Hz}$, $-\text{CH}$), 4.1 (d, $J = 4.09$, $-\text{CH}$), 6.55 (m, $J = 5.20$, $-\text{CH}$), 7.22 (m, $J = 3.63\text{Hz}$, $-\text{CH}$), 7.45 (t, $J = 2.75\text{Hz}$, $-\text{CH}$), 7.68 (d, $J = 1.19\text{Hz}$, $-\text{CH}$), 8.81 (s, $J = 3.19\text{Hz}$, $-\text{CH}$). ^{13}C NMR (400 MHz, $\text{DMSO}-d_6$) 18.25, 19.30, 30.78, 32.07, 59.58, 71.34, 72.59, 117.70, 118.18, 121.76, 135.35, 135.48, 164.23, 165.02. FT-IR (KBr, cm^{-1}) 3415, 2958, 1618, 1275, 1075, 1025. Elemental Anal. Calc. for $\text{C}_{18}\text{H}_{29}\text{NO}_4\text{Ti}$: C, 58.23; H, 7.87; N, 3.77; O, 17.24; Ti, 12.89. Found: C, 57.11; H, 7.28; N, 3.87;

2.4 ROP reaction of ϵ -CL

The polymerization reactions were carried out in an Ace pressure tube in the presence of pure nitrogen atmosphere with the homogeneous heating. 0.005 g (0.014 mmol) of catalyst (LVTi) has been added to 0.97 ml (1.0 g, 8.8 mmol) of ϵ -CL and the obtained mixture was heated at 125°C under N_2 atmosphere for 24 h (Scheme 2). Succeeding the completion of the reaction, the product was later dissolved in 10 mL of chloroform and centrifuged. The obtained solution was poured into an excess of methanol. The white precipitate (PCL) obtained was filtered separately then washed several time using methanol and dried for 8–10 h in vacuum. Yield 0.96 g (96%), $M_w = 42,000$. IR (KBr disc, cm^{-1}): 1727 ($-\text{C}=\text{O}$), 2864 ($-\text{CH}_2$), 2942 ($-\text{CH}_2$), 3433 ($-\text{OH}$). ^1H NMR (CDCl_3 , δ ppm): 2.30 (t, 2H, $-\text{CH}_2$), 1.65 (m, 2Hs, $-\text{CH}_2$), 1.40 (m, 2H, $-\text{CH}_2$), 4.04 (t, 2H, $-\text{CH}_2$).

Scheme 2 LVTi catalyzed ROP reaction of ϵ -CL

2.5 Synthesis of BiFeO_3 NPs:

The synthesis procedure followed for BFO NPs is similar to the one found in the literature.²⁹ The synthesis procedure is as follows. $\text{Bi}(\text{NO}_3)_3 \cdot 5\text{H}_2\text{O}$ and $\text{Fe}(\text{NO}_3)_3 \cdot 9\text{H}_2\text{O}$ combination has been dissolved in 200 mL of double distilled water and stirred well for 20 minutes to obtain a clear solution. The reaction product is obtained by adding the synchronized drops of the mixture which includes the ammonia solution and distilled water. This precipitate was then maintained at room temperature for about 24 hours and then washed several times with double distilled water to remove the unreacted products and then filtered. Afterwards the final product was dried in hot air oven at 100°C for about 5 hours. At last, the final sintering has been carried out at 600°C for 2 hours.

2.6 Synthesis of PCL/ BiFeO_3 nanocomposite materials.

PCL/BFO NPs nanocomposites were prepared by solution casting method with different weight percentage of BFO NPs contents (1

and 3wt %). PCL and BFO NPs were weighed, and dissolved in 30 mL chloroform, later it has been stirred for 30 minutes at room temperature. These solutions were mixed and stirred for 1 hour to obtain the homogeneous solution. As well, the solution mixture has been casted in a glass Petri dish and dried at the solvent atmosphere to obtain solid sample. The obtained nanocomposite has been characterised by various techniques such as FE-SEM, XRD and DSC.

3. Results and Discussion

3.1 Characterization of catalyst

The chiral Schiff base ligand has been synthesized by reacting L-valinol with salicylaldehyde, following the literature procedure.²⁵ The titanium complex LVTi has been prepared by reacting one equivalent of the metal precursor $\text{Ti}(\text{O}^i\text{Pr})_4$ with the same equivalent of the corresponding ligand (LV) (Scheme 1). UV spectral studies provided the below useful insights in the complex formations. The recorded spectra for LV and LVTi were shown in the Fig. 1. From Fig. 1, it has been observed that the pure LV exhibits two intensive bands at $38,760\text{ cm}^{-1}$ and $31,646\text{ cm}^{-1}$ which confirms the $\pi-\pi^*$ and $n-\pi^*$ transitions. However LVTi shows an intense band with an observable blue shift at ($39,062\text{ cm}^{-1}$) and the formation of new broad band appears around ($27,642\text{ cm}^{-1}$). This observation attributes to charge transfer from metal to ligand (MLCT) transitions which was identified. The consequence of coordination in the metal confirms the formation of LVTi complex which makes the shift towards shorter wavelength.

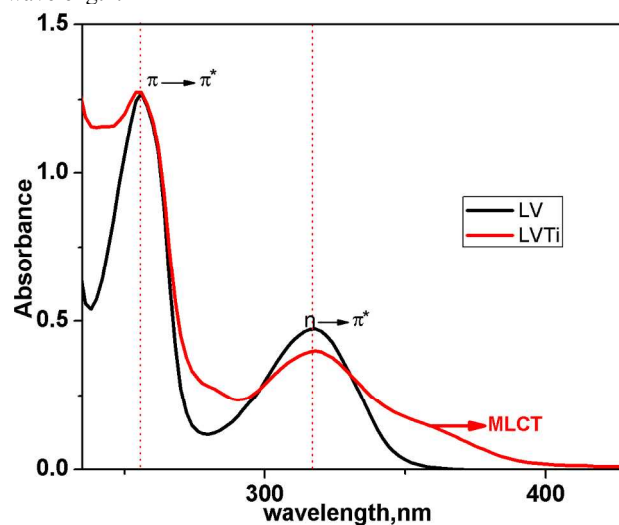


Fig. 1 UV-Visible spectrum of pure LV and LVTi.

In order to confirm the structure of the synthesized complex, ^1H & ^{13}C NMR spectrum was also measured. The obtained results signifies the co-ordination of metal Ti via hydroxyl-OH group and azomethine($-\text{CH}=\text{N}-$)group. All the protons were shifted downfield after complexation. Interestingly it has been observed that the hydroxyl-OH protons disappear during the complex formation. Moreover the azomethine proton of LV (8.29ppm) suffers a significant downfield shift (8.9) upon coordination to Ti (IV) metal ion. Infact the azomethine proton were deshielded being responsible for the observed downfield shift. Furthermore, the peaks due to methyl and methane protons of isopropyl groups ($\text{Ti}-\text{O}-\text{CH}(\text{CH}_3)_2$) are detected at 0.9–1.2 ppm (doublets) and 4.7 ppm (septets) respectively. The complex formation has been further confirmed by ^{13}C NMR spectrum as follows.

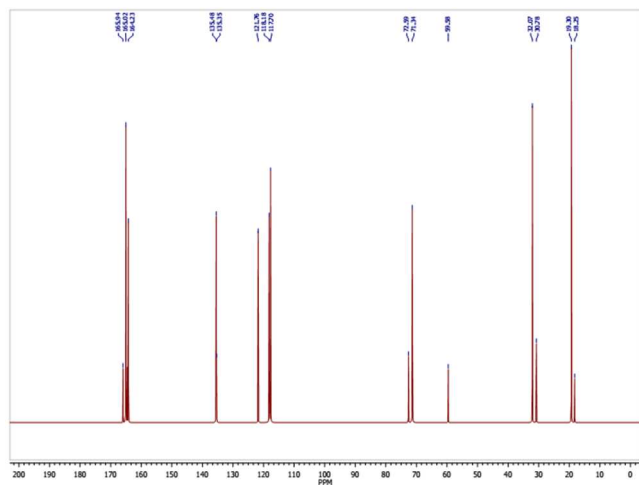


Fig. 2 ^{13}C NMR spectrum of LVTi

In ^{13}C NMR spectrum of LVTi, the two aliphatic carbon peaks of newly formed isopropyl groups are observed at 30 and 59 ppm (Fig. 2). Five aromatic carbon peaks are shown in the range 115-135 ppm and the remaining peak at δ 164 ppm is attributed to oxygen attached quaternary carbon (C-O) which is shift into downfield region than their corresponding ligand (δ 151 ppm). This is in good agreement for complex formation. Finally the azomethine carbon is shifted from 161 ppm to 165 ppm. These statistics clearly reveals the complex formation.

Table 1 Optimization of reaction conditions for the synthesis of PCL

Entry	[M]/[C] ^a ratio	Temperature (°C)	Time (h)	$M_n^b \times 10^3$ (g/mol)	$M_w^c \times 10^3$ (g/mol)	Yield ^d (%)	PDI ^e
1	–	150	24	–	–	–	–
2	653:1	150	24	31.66	42.12	96	1.33
3	653:1	150	12	20.60	31.73	95	1.54
4	653:1	150	6	12.61	21.52	90	1.70
5	1308:1	150	24	27.38	36.00	95	1.31
6	1308:1	150	12	13.79	16.79	92	1.21
7	1308:1	150	6	7.81	12.33	90	1.57
8	2612:1	150	24	14.11	22.71	92	1.60
9	2612:1	150	12	7.08	11.32	90	1.59
10	2612:1	150	6	4.72	9.41	87	1.99
11	3265:1	150	24	9.40	15.15	93	1.61
12	3265:1	150	12	6.03	9.10	91	1.50
13	3265:1	150	6	3.97	4.82	86	1.21
14	653:1	125	24	22.96	34.55	94	1.50
15	1308:1	125	24	19.55	31.98	90	1.63
16	2612:1	125	24	9.20	13.07	91	1.42
17	3265:1	125	24	7.24	11.53	86	1.59
18	366:1 ^{a*}	150	24	1.46	1.77	74	1.20
19	517:1 ^{a**}	150	24	6.31	9.83	84	1.55

^a [M]/[C] ratio is the molar ratio of monomer and catalyst.

^{a*} [M]/[C] ratio is the molar ratio of monomer and Ligand (LV).

^{a**} [M]/[C] ratio is the molar ratio of monomer and $\text{Ti}(\text{O}^i\text{Pr})_4$.

^b M_n is the relative number-average molecular weight.

^c M_w is the relative weight-average molecular weight.

^d Calculated on the basis of the polymer weight.

^e $\text{PDI} = M_w/M_n$.

3.2 Optimization of reaction condition for ROP reaction of ϵ -CL.

The chiral LVTi Schiff base complex has been used as catalyst for ROP of ϵ -CL under solvent free conditions. To optimize the reaction conditions, polymerization reaction was carried out with different amount of catalysts such as 5, 2.5, 1.5 and 1 mg. The temperatures are kept at 150 and 125 °C for, various duration of reaction time such as 6, 12 and 24 h. The obtained results for PCL synthesis at these different conditions were given in table 1. Optimum conditions of reaction temperature, reaction time and catalyst amount were maintained at 150 °C, 24h and 5 mg (table 1, entry 2) for LVTi catalyst. For comparison, the same polymerization reactions has been carried out with pure LV (table 1, entry 18), $\text{Ti}(\text{O}^i\text{Pr})_4$ (table 1, entry 19) and blank (table 1, entry 1) and they showed an inferior catalytic performance as opposed to their LVTi.

The ^1H NMR spectrum of PCL (Fig. 3) showed a significant signal at δ 3.66 (triplet) corresponding to the $-\text{CH}_2-\text{OH}$ end group in PCL. Two signals at 1.35 and 4.2 were also observed for PCL due to the presence of methyl ester end group. ^{13}C NMR (CDCl_3 , δ , ppm): 34.12 ($-\text{CH}_2$), 28.34 ($-\text{CH}_2$), 24.57 ($-\text{CH}_2$), 25.52 ($-\text{CH}_2$), 64.16 ($-\text{CH}_2$), 173.58 ($-\text{C}=\text{O}$) showed respective number of carbons at appropriate regions

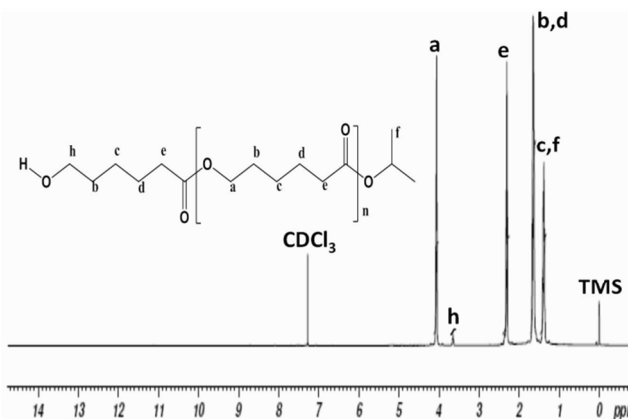


Fig. 3 ^1H NMR spectrum of PCL synthesized by ROP method using LVTi complex and illustrating the end group analysis.

3.3 Characterization of nanocomposites.

DSC was measured in the temperature range between 30 – 250°C for pure PCL and PCL blended with BFO samples. It was observed that the melting temperature of PCL and PCL/BFO/3wt% nanocomposite is 55°C and 58°C respectively. The observed increase of the melting temperature (T_m) of PCL/BFO/3wt% is attributed to the addition of BiFeO_3 NPs assist to produce crystallization grain and form a more regular structure in PCL. Hence, T_m of nanocomposites is elevated a bit compared with that of PCL matrix, and the melting peak follow off with increasing PCL/BFO/3wt% content. Moreover, it can also be considered that, the inorganic grains BFO added into the system PCL, hinder the large movement of PCL long chains and it is inconvenient for chains to move freely to change the configuration³¹. Both of these two factors and their synergistic effect result to the shift of T_m in PCL/BFO/3wt% nanocomposite. The X-ray diffraction pattern of pure PCL, pure BFO NPs, PCL/BFO/1 wt% and PCL/BFO/3 wt% nanocomposites shows the crystalline behaviour in Fig.4 PCL sample, shows three crystalline peaks at 21.08°, 21.87°, and 23.34° corresponds to (110), (111), and (200) planes.

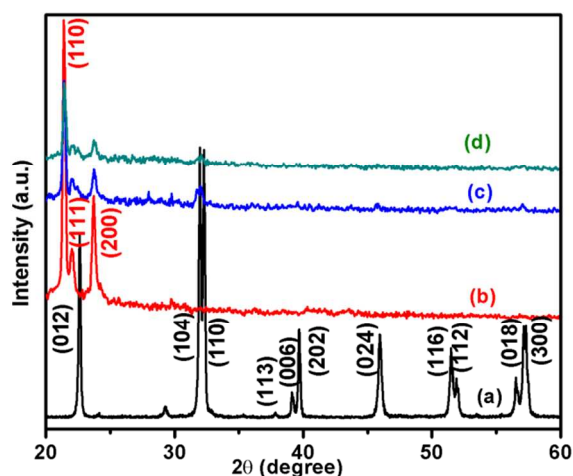


Fig.4 X-ray diffraction pattern of (a) BFO Nps, (b) PCL, (c) PCL/BFO/ 1 wt%, (d) PCL/BFO/ 3wt%.

This demonstrates a highly ordered chain folding characteristics of the sample.³⁰BFO NPs exhibit a single-phase structure, and the diffraction peaks are indexed to be the rhombohedral BiFeO₃ with space group *R3c* (JCPDS card no. 71-2494). XRD data was collected at a slow scan rate of 0.05°/min. The pure BFO NPs diffractogram shows sharp peaks at 22.6°, 31.8, 32.12°, 39.75°, 45.95°, 51.45° and 57.25° corresponds to (012), (104), (110), (202), (204), (116) and (500). This depicts their highly crystalline nature.²⁹ As well the XRD pattern of PCL/BFO/1 wt% and PCL/BFO/3 wt% nanocomposite peaks were destabilized when compared with pure PCL and pure BFO NPs. This confirms the formation of nanocomposites.

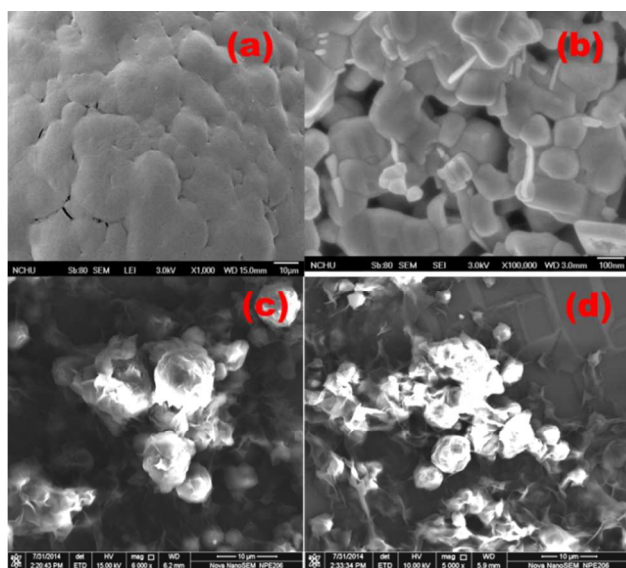


Fig. 5 SEM micrographs of (a) PCL, (b) BFO Nps, (c) PCL/BFO/ 1%, (d) PCL/BFO/ 3%.

FE-SEM image shows one of the evidence for formation of the nanocomposites. The FE-SEM microstructure and morphology of (a) PCL, (b) BFO NPs, (c) PCL/BFO/1 wt% and (d) PCL/BFO/3 wt% nanocomposites in the same scale of 10 μm were shown in Fig. 5. Cloud like appearance is observed for PCL microstructure and (b) shows a pure BFO NPs average size of 100 nm. NPs has been homogeneously and compactly dispersed in the PCL atmosphere to form glans penis structure. As shown in Fig. 5 (c

& d), PCL/BFO/1 & 3 wt%, the composites showed more homogeneous, well stretched and with the single phase morphology. This demonstrates the good interaction of components in the matrix.

3.4 Dielectric and electric modulus properties

Dielectric properties studies are important to understand the nature and the origin of dielectric losses, which, in turn, may be useful in the determination of structure and defects in solids. The real part of dielectric constant is derived from the following relation,

$$\epsilon'(\omega) = \frac{Cd}{\epsilon_0 A} \quad \text{-----} \quad (1)$$

Where *C*, is the measured capacitance in Farad, *d* and *A* correspond to thickness and cross sectional area of the pellets in meter and m² respectively, $\epsilon_0 = 8.85 \times 10^{-12}$ F.m⁻¹ is the permittivity of free space.

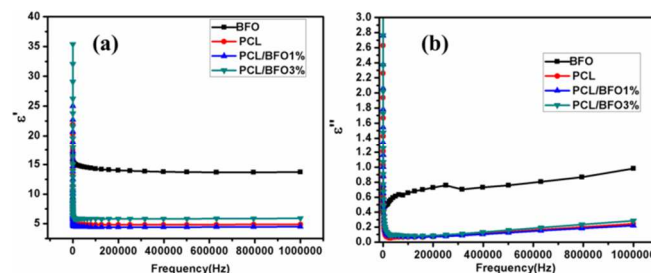


Fig. 6 Frequency dependence of the (a) dielectric constant and (b) dielectric loss.

The frequency dependence of dielectric constant ϵ' and dielectric loss ϵ'' at room temperature at the frequency range from 100 Hz to 1MHz measured samples were shown in Fig. 6. It has been observed that the prepared BFO NPs has higher dielectric constant values compared to prepared PCL/BFO/1wt% and PCL/BFO/3wt%. This may be attributed to the space charge polarization near the grain boundary which depends on the high purity and perfections of the sample.

Also dielectric constant and dielectric loss values decreases gradually as the frequency increased from lower frequency and then become almost constant up to 1MHz for all the sample values. These observations may be explained by the phenomenon of dielectric dispersion evidently. Such a strong dispersion seems to be a common feature in ferroelectric materials concerned with ionic conductivity, which is referred to as low-frequency dielectric dispersion.^{32,33}

The dielectric properties of materials can be expressed in various ways, with different representations. Although these alternative representations are equally valid, they may often provide new insight into the dielectric and electrical properties of materials. Therefore, many researchers prefer to describe the dielectric properties by using the electric modulus formalism.

The complex electric modulus has been derived from the complex permittivity,³⁴ according to the relationship defined by Macedo et al.³⁵ The complex electric modulus was calculated from the complex permittivity. The real (M') and imaginary (M'') parts of the electric modulus can be calculated from ϵ' and ϵ'' as follows:

$$M' = \frac{\epsilon'}{\epsilon'^2 + \epsilon''^2} \quad \text{-----} \quad (2)$$

$$M'' = \frac{\epsilon''}{\epsilon'^2 + \epsilon''^2} \quad \text{-----} \quad (3)$$

The frequency dependence of the complex modulus spectrum (M' and M'') of BFO, PCL, PCL/BFO/1wt% and PCL/BFO/3wt % nanocomposite is shown in Fig. 7 (a), (b). BFO has been characterized by very low value (almost zero) of M' and M'' in the frequency region 1KHz-1MHz.

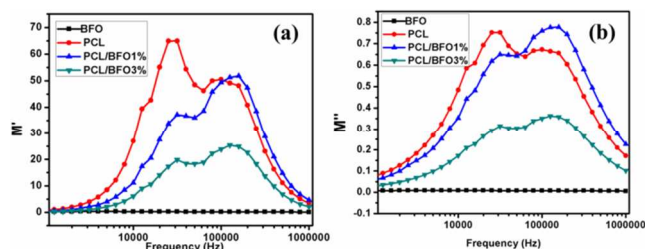


Fig. 7 Frequency dependence of the electric modulus, (a) M' (b) M'' .

The variation of M' with frequency of PCL, PCL/BFO/1wt% and PCL/BFO 3wt% nanocomposites, result in the initial increase of magnitude of electric modulus with an increase in frequency, afterwards a fall in electrical modulus is observed. This attributed to the presence of conduction phenomena due to short-range mobility of charge carriers.³⁶ Variation of M'' as a function of frequency for all the nanocomposites is shown in Fig. 7(b). The width of M'' peak was found to be increased with increase in frequency and its magnitude decreases with increasing BFO NPs suggesting enhancement in the capacitance of nanocomposites. The observation of two maximum peaks, the first peak at lower frequency corresponds to the capacitance of grain boundaries and the second peak at higher frequency corresponds to grains capacitance.

3.5 Impedance spectra and ac conductivity

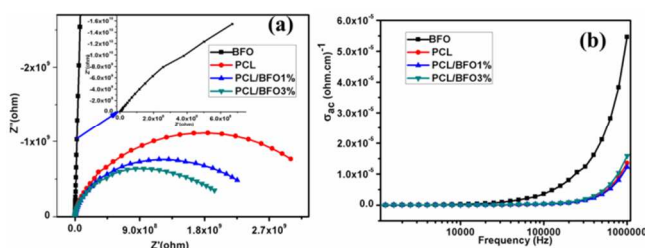


Fig. 8(a) Plot of the imaginary part and real part of impedance and (b) Variation of AC conductivity with respect to frequency.

The complex impedance measurements of AC conductivity were done based on studies made on measurements of cell impedance. This is shown by plotting the relation between Z (impedance), and Y (admittance) in complex plane which is known as Nyquist diagram

$$Z = Z' + Z'' \quad (4)$$

Where Z' and Z'' are the real and imaginary parts of impedance Z , respectively:

$$Z' = |Z| \cos \theta \quad (5)$$

$$Z'' = |Z| \sin \theta \quad (6)$$

In general, Z for both parts is frequency dependent. Impedance spectroscopy consists of the measurement of $Z(\omega)$ over a widerange frequency. The relation between imaginary part (Z'') and real part (Z') are plotted in the Fig. 8. It was observed that the

magnitudes of both Z' and Z'' were decreased with increase in frequency. This indicates the increase in ac conductivity with rise in higher frequency.

When the impedance for BFO NPs sample is very high, the impedance plot (inset graph (8)) shows a straight line and not semicircular arc curve over the measured frequency region. Only single semicircle could be traced at room temperature for PCL, PCL/BFO 1wt%, PCL/BFO 3wt% nanocomposites. As BFO NPs mixed with polymer samples, the diameter for impedance plots becomes decreased. This demonstrates the decreased impedance for all nanocomposites.

The AC conductivity (σ) was calculated by the following equation³⁷

$$\sigma = \epsilon_0 \epsilon'' \omega \tan \delta \quad (7)$$

The variation of ac conductivity with frequency for all the samples is shown in Fig.8. BFO NPs, PCL, PCL/BFO 1% and PCL/BFO 3wt% nanocomposites shows increase of AC electrical conductivity with increase in frequency. For all the nanocomposite samples, the ac conductivity values are same at low frequencies and further increase in conductivity was observed after 15 kHz is attributed to atomic and electronic polarizations.^{38,39} It is clear from these observations that the ac conductivity value of BFO NPs is found to be one order (in magnitude) less than of PCL, PCL/BFO/1wt% and PCL/BFO/3wt% samples.

3.6 The leakage current density

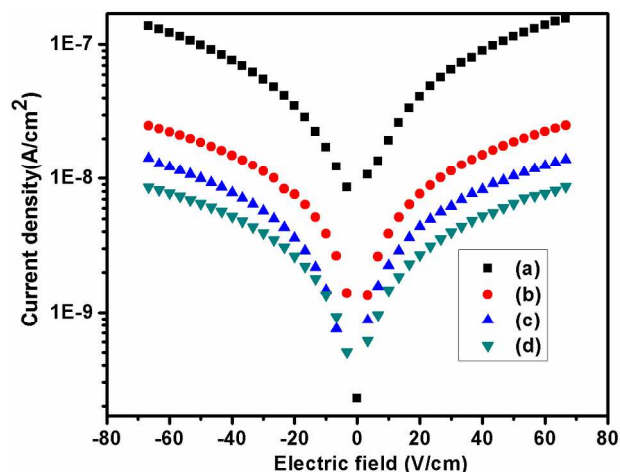


Fig. 9 Electric field dependence of leakage current density (J-E) of (a) BFO Nps, (b) PCL, (c) PCL/BFO/ 1%, (d) PCL/BFO/ 3%.

To investigate the leakage behaviour Fig. 9 (a), (b), (c) and (d) of the prepared pure BFO NPs, pure PCL, PCL/BFO/1wt% and PCL/BFO/3wt% the samples were subjected to the electric field up to ± 90 V/cm at room temperature. It signifies that current density increased with increase in electric field for all the compositions. The leakage current was then observed for both the forward and reverse bias conditions attributed to the bulk-limited conduction in BFO ceramics. The leakage current in BFO is usually attributed to the space charges (such as oxygen vacancies) induced mainly by Bi volatilization.⁴⁰ At an applied electric field of 65 V/cm, the leakage current density of PCL/BFO/3wt% is about 1.3×10^{-7} A/cm² which is approximately one order of magnitude less than that of PCL and BFO NPs.

3.7 Ferroelectric properties

The electric field dependent polarization measurement for the prepared pure BFO NPs, pure PCL, PCL/BFO/1wt% and PCL/BFO/3 wt% samples has been performed at two different frequencies and are shown in Fig. 10 (a), (b), (c) and (d). The values of remnant polarization for the prepared pure BFO NPs, pure PCL, PCL/BFO/1 wt% and PCL/BFO/3 wt% samples at 500 Hz are 0.025, 0.011, 0.089 and 0.122 $\mu\text{C}/\text{cm}^2$, respectively. This enhancement of remnant polarization occurs with the increasing BFO NPs blended with PCL samples. It has been found that the hysteresis loops of BFO ceramics become slimmer with the increasing of frequency, which indicates that the remnant polarization and the coercive electric field decreases as frequency increases. At low frequency, there were electron displacement, ion displacement, turning-direction polarization and space charge polarization observation in BFO. But as frequency increases, the space charge polarization would not keep up with change of electric field so that the remnant polarization and the coercive field tends to decrease.⁴¹

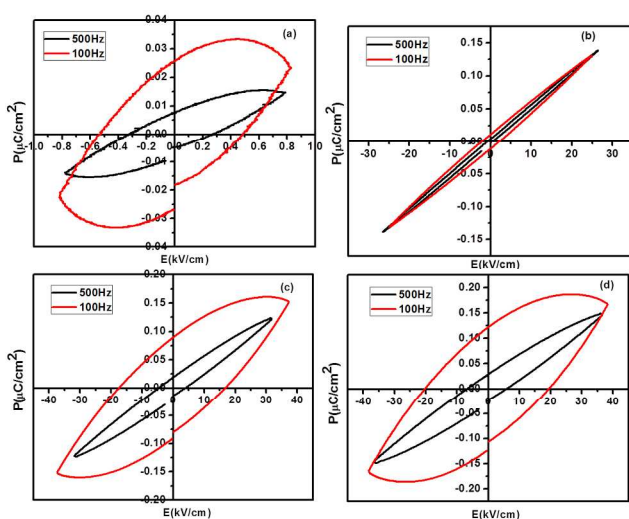


Fig. 10 Polarization versus electric field (P-E) hysteresis loops of a) BFO Nps, (b) PCL, (c) PCL/BFO/ 1%, (d) PCL/BFO/ 3% samples measured at different frequencies.

4. Conclusions

In summary, we can assure that this is the first report in the study of BFO NPs blended with PCL along with their comparative study for the prepared pure BFO NPs, PCL, PCL/BFO/1 wt% and PCL/BFO/3 wt% nanocomposites. The chiral LVTi complex has been successfully synthesized and structurally characterized. The characterized LVTi complex has been used as an efficient catalyst for ROP of ϵ -CL by applying the solvent free process method. The prepared nanocomposite PCL/BFO/1 wt%, PCL/BFO/3 wt% has its own significant impact for the ferroelectric and reduction of leakage current density properties. Moreover, the remnant polarization of the nanocomposites increases when being compared with that of the pure BFO NPs. AC conductivity of BFO NPs is found to be one order (in magnitude) less than of PCL, PCL/BFO/1wt% and PCL/BFO/3wt% samples.

Acknowledgment

The authors gratefully acknowledge funding support from the Council of Scientific & Industrial Research (CSIR) Sanction No.

45 01(2282)/08/EMR-II. DST (Sanction No: SR/S1/OC-06/2011) for providing GPC facility for molecular weight characterization.

Notes and References

a. Organic and Polymer Synthesis Laboratory, Department of Chemistry, National Institute of Technology, Tiruchirappalli 620 015, India

b. Advanced Functional Materials Laboratory, Department of Physics, National Institute of Technology, Tiruchirappalli 620 015, India

*Corresponding author. Tel.: +91 431 2503640; fax: 91 431 2500133. E-Mail address: velmathis@nitt.edu (S. Velmathi).

1. L. Yu, K. Dean, and L.Li, *Prog.Polym.Sci.*2006, **31**, 576-602.
2. H. Y. Kweon, M. K. Yoo, K. Park, T. H. Kim, H. C. Lee, H. S. Lee, *Biomaterials*, 2003, **24**, 801-808.
3. J. P. Jain, M. Sokolsky, N. Kumar, A.J. Domb, *Polym. Rev.* 2008, **48**, 156-191.
4. M. Labet, W. Thielemans, *Chem. Soc. Rev.* 2009, **38**, 3484-3504.
5. M. Okada, *Prog. Polym. Sci.* 2002, **27**, 87-133.
6. J.H. Khan, F. Schue, G.A. George, *Polym. Int.*58, **2009**, 296.
7. G.W.V Cave, C.L. Raston, Scott JL, *Chem. Commun.*21, **2001**, 2159.
8. N. Nomura, T. Aoyama, R. Ishii, T. Kondo, *Macromolecules*. 2005, **38**, 5363-5366.
9. Y. Takashima, Y. Nakayama, K. Watanabe, T. Itono, N. Ueyama, A. Nakamura, H. Yasuda, A. Harada, *Macromolecules*. 2002, **35**, 7538-7544.
10. A. Kowalski, J. Libiszowski, T. Biela, M. Cypryk, A. Duda, S. Penczek, *Macromolecules*. 2005, **38**, 8170-8176.
11. M. Vivas, J. Contreras, *Eur. Polym. J.* 2003, **39**, 43-47.
12. H. J. Chuang, H. L. Chen, J. L. Ye, Z.Y. Chen, P. L. Huang, T. T. Liao, T. E. Tsai and C. C. Lin, *J. Polym. Sci., Part A: Polym. Chem*, 2013, **51**, 696-707,
13. D. Deivasagayam, F. Peruch, *Polymer*. 2011, **52**, 4686-4693.
14. K.C. Gupta, A.K. Sutar, *Coord. Chem. Rev.* 2008, **252**, 1420-1450.
15. D.A. Atwood, M.J. Harvey, *Chem. Rev.* 2001, **101**, 37-52.
16. H.S. Nalwa, *Handbook of Low and High Dielectric Constant Materials and Their Applications*; Academic Press: London, 1999.
17. Y.B. Cohen, *Electroactive Polymer (EAP) Actuators as Artificial Muscles*; SPIE Press: Bellingham, WA, 2004.
18. Q.M.Zhang, V.Bharti, X. Zhao, *Science* 1998, **280**, 2101-2104.
19. G.Lu, X.Li, H.Jiang, X. Mao, *J. Appl. Polym. Sci.* 1996, **62**, 2193-2199.
20. C.W. Nan, *Prog. Mater. Sci.* 1993, **37**, 1-116.
21. D.K. Das-Gupta, *Ferroelectric Polymer and Ceramic-Polymer Composites*; Trans Tech: Aedermannsdorf, Switzerland, 1994.
22. V. Tomer, E.Manias, C. A. Randall, *J. Appl. Phys.* 2011, **110**, 044107.
23. W. Prellier, M. P.Singh, P. Murugavel, *J. Phys.: Condens. Matter*. 2005, **17**, 803-832.

24. M. Fiebig, *J. Phys. D: Appl. Phys.* 2005, **38**, 123–152.
25. S.Roy, R.Chatterjee, S. B. Majumder, *J. Appl. Phys.* 2011, **110**, 036101.
26. A.V. Reddy, K.C.Sekhar, N.Dabra, A.Nautiyal, J. S.Hundal, N. P.Pathak, R. Nath, *ISRN Mater. Sci.* 2011, **5**, 142968.
27. N. Ananthi, U. Balakrishnan, S. Velmathi, *ARKIVOC*, 2010, **ix**, 370.
28. M. Hayashi, Y. Miyamoto, T. Inoue, N. Oguni, *J. Org. Chem.* 1993, **58**, 1515-1522.
29. M. Muneeswaran, P. Jegatheesan, M. Gopiraman, I. S. Kim, and N.V. Giridharan, *Appl. Phys. A.* 2014, **114**, 853–859.
30. A. Elzubair, C.N. Elias, J.C.M. Suarez, H.P. Lopes, M.V.B. Vieira, *J Dent.* 2006, **34**, 784–789.
31. J. Ren, T. Yu, H. Li, T. Ren, S. Yang, *POLYM. COMPOS*, 2008, **29**, 1145–1151.
32. J.R. Teague, R. Gerson, and W.J. James, *Solid State Commun.* 1970, **8**, 1073–1074.
33. X.X. Wang, S.H. Choy, X.G. Tang, and H.L.W. Chan, *J. Appl. Phys.* 2005, **97**, 104101–104104.
34. B.G. Soares, M.E. Leyva, G.M.O. Barra, D. Khastgir, *Eur. Polym. J.* 2006, **42**, 676-686.
35. P.B. Macedo, C.T. Moynihan, R. Bose, *Phys. Chem. Glasses.* 1972, **13**, 171-179.
36. P.S. Das, P.K. Chakraborty, B. Behera, R.N.P. Choudhary, Electrical properties of $\text{Li}_2\text{BiV}_5\text{O}_{15}$ ceramics, *Phys. B Condens. Matter.* 2007, **395**, 98-103.
37. Z. Peng, Q.Chen, J. Wu, D. Liu, D. Xiao, J. Zhu. *J. Alloy Compd.* 2012, **541**, 310–316.
38. P. Smyth, *Dielectric Behavior and Structure*, McGraw-Hill, New York, 1965.
39. M. Barsoum, *Fundamental of Ceramics*, McGraw-Hill, New York, 1997.
40. S. Zhang, L. Wang, Y. Chen, D. Wang, Y. Yao, Y. Ma, *J. Appl. Phys.* 2012, **111**, 074105.
41. W. Cai, C.L. Fu, Z.B. Lin, X.L. Deng, *Ceram. Int.* 2011, **37**, 3643-3650.